nature genetics

© 2004 Nature Publishing Group http://www.nature.com/naturegenetics

In situ analyses of genome instability in breast cancer

Koei Chin[1,6], Carlos Ortiz de Solorzano[2,6], David Knowles[2], Arthur Jones[3], William Chou[2], Enrique Garcia Rodriguez[2], Wen-Lin Kuo[1], Britt-Marie Ljung[4], Karen Chew[1], Kenneth Myambo[1], Monica Miranda[1], Sheryl Krig[2], James Garbe[2], Martha Stampfer[2], Paul Yaswen[2], Joe W Gray[1,2,6] & Stephen J Lockett[2,5,6]

Transition through telomere crisis is thought to be a crucial event in the development of most breast carcinomas. Our goal in this study was to determine where this occurs in the context of histologically defined breast cancer progression. To this end, we assessed genome instability (using fluorescence *in situ* hybridization) and other features associated with telomere crisis in normal ductal epithelium, usual ductal hyperplasia, ductal carcinoma *in situ* and invasive cancer. We modeled this process *in vitro* by measuring these same features in human mammary epithelial cell cultures during *ZNF217*-mediated transition through telomere crisis and immortalization. Taken together, the data suggest that transition through telomere crisis and immortalization in breast cancer occurs during progression from usual ductal hyperplasia to ductal carcinoma *in situ*.

The molecular events that enable normal epithelial cells to progress to invasive, metastatic disease are increasingly well understood[1,2]. Deregulation of the *TP53* and *RB1* pathways in most cancers enables extended proliferation. In breast cancer, deregulation of *RB1* through inactivation of cyclin-dependent kinase inhibitor 2A (*CDKN2A*, also called *p16* and *INK4a*) seems to be an early event[3]. Most epithelial cells

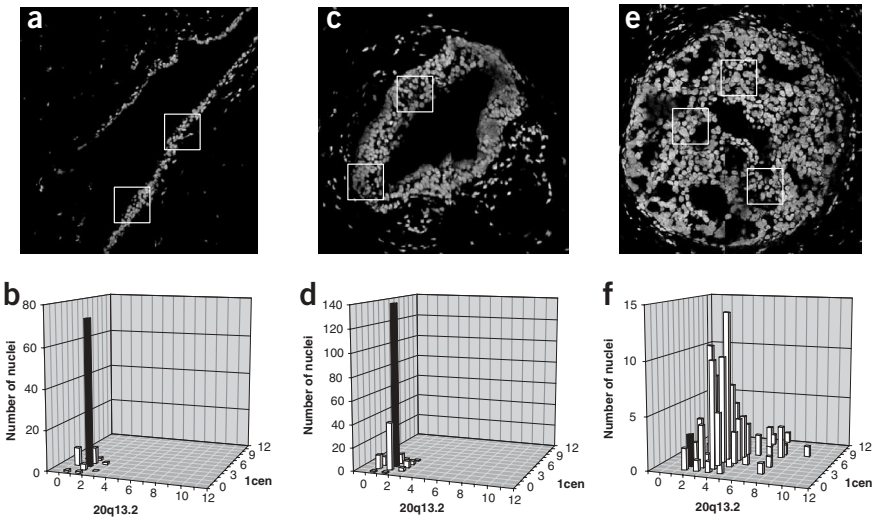

Figure 1 2D confocal YO-PRO-1 images and bivariate copy-number histograms of chromosome 1cen and 20q13.2 signals in 3D images. Open bars indicate the numbers of cells with copy numbers specified on the *x* and *y* axes. Filled bars indicate the number of cells with two copies each of 1cen and 20q13.2. (**a**) A 2D confocal YO-PRO-1 image of normal ductal epithelium taken midway through a 30-μm-thick tissue section. The white squares (100 μm × 100 μm) indicate regions for which 3D confocal images were acquired for copy-number analysis. (**b**) A bivariate copy-number frequency histogram of the number of copies of 1cen and 20q13.2 in the regions indicated in **a**. More than 90% of nuclei had two copies of 1cen and 20q13.2. Statistical analysis of measurements on 537 nuclei from several normal specimens indicated that 93 ± 4% of genuine FISH signals were detected and that there was a 4 ± 4% chance that a detected signal was spurious (**Supplementary Table 1** online). (**c**) A 2D confocal YO-PRO-1 image of a UDH. (**d**) A bivariate frequency histogram of 1cen and 20q13.2 copy numbers measured for the regions indicated in **c**. Most cells had two copies of 20q13.2, but 22% of cells had only one copy of 1cen. (**e**) A 2D confocal YO-PRO-1 image of a DCIS showing an expanded duct filled with heterogeneous tumor cells. (**f**) A bivariate frequency histogram of 1cen and 20q13.2 copy numbers measured for the regions indicated in **e** showing substantial genomic instability. DNA content was associated with genome copy number measured using FISH in this sample (correlation coefficient = 0.83; 89 data pairs).

[1]Department of Laboratory Medicine and Comprehensive Cancer Center, University of California San Francisco, California, USA. [2]Life Sciences Division and [3]Engineering Division, Lawrence Berkeley National Laboratory, Berkeley, California, USA. [4]Department of Pathology and Comprehensive Cancer Center, University of California San Francisco, California, USA. [5]Present address: SAIC-Frederick, P.O. Box B, Frederick, Maryland, USA. [6]These authors contributed equally to this work. Correspondence should be addressed to J.W.G. (jwgray@lbl.gov).

Published online 8 August 2004; doi:10.1038/ng1409

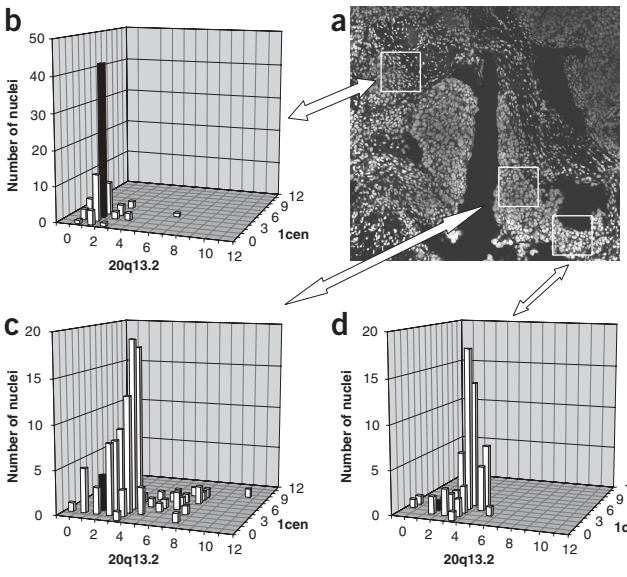

Figure 2 A 2D YO-PRO-1 image and bivariate copy number histograms of chromosome 1cen and 20q13.2 signals from an invasive cancer. Open and filled bars are as defined in **Figure 1**. (**a**) A 2D YO-PRO-1 image showing tumor cells invading the stroma beyond the basement membrane. The white squares indicate regions for which 3D images were acquired and analyzed for copy number. (**b–d**) Bivariate frequency histograms of 1cen and 20q13.2 copy numbers measured for the regions indicated in **a**. Some regions had near-normal copy numbers (**b**), but others had high copy-number variability (**c**,**d**). DNA content and nuclear volume were nearly normal for the cells in **b** and increased for the cells in **c** and **d**.

lack active telomerase, and so extended proliferation leads to telomere erosion and, eventually, loss of telomere function[4]. These cells become genomically unstable[5] and are almost always eliminated by damage-surveillance mechanisms[5–7]. Rarely, however, one or a few cells escape this protective mechanism by reactivating telomerase[7] and develop additional cancer hallmarks[2] through accumulation of multiple genomic and epigenomic aberrations[8]. Thus, telomere crisis, defined in this paper as the events that occur when cells lose telomere function as a result of extended proliferation in the absence of telomerase, is a critical rate-limiting and promoting event[1].

Several features of breast cancer suggest that telomere crisis occurs in breast cancer during transition from usual ductal hyperplasia (UDH) to ductal carcinoma *in situ* (DCIS). First, the total number of aberrations typically is much higher in DCIS than in UDH[9]. This increase is reminiscent of the increase in genome aberrations in tumors that arise in late-generation telomerase-knockout mice[1]. Second, progressive shortening of telomeres[10] and reactivation of telomerase occurs during transition from UDH to DCIS[11]. If transition through telomere crisis does occur during transition from UDH to DCIS, genome instability should increase substantially during this transition. We assessed this possibility by measuring genome instability (using fluorescence *in situ* hybridization, FISH), DNA content and telomere length at several histologically distinct stages of breast cancer progression. We compared these features with those observed in cultured human mammary epithelial cells (HMECs) during transition through *ZNF217*-mediated telomere crisis and immortalization[12].

We assessed instability by three-dimensional (3D) confocal microscopic analysis of ~30-μm-thick tissue sections stained for copy number using dual-color FISH[13] with probes for the centromere of chromosome 1 (1cen) and chromosome 20q13.2 and with the DNA-specific dye YO-PRO-1. We analyzed three-color (DNA stain and two FISH probe labels), 3D images generated using confocal microscopy in regions of histological interest to determine the boundaries and volumes of intact nuclei and to enumerate dual-color FISH signals therein (**Supplementary Fig. 1** online). We used the standard deviation of the number of the FISH signals (σ_{CN}) as a quantitative measure of genome instability. We obtained histological information from YO-PRO-1 images and confirmed it in some cases by microscopic analysis of adjacent thin sections stained with hematoxylin and eosin (**Supplementary Fig. 2** online).

We measured genome instability and DNA content in normal human skin, normal breast epithelium and stroma, three UDH specimens, three DCIS specimens and four invasive cancer specimens (**Figs. 1–3**). One sample of normal epithelium had low instability ($\sigma_{CN} = \sim 0.5$; **Fig. 1a**,**b**), as did one UDH specimen ($\sigma_{CN} = \sim 0.6$–0.7; **Fig. 1c**,**d**). Most cells had two copies of 20q13.2, but a significant fraction (22%, $P < 0.001$) had only one copy of 1cen. Spatial

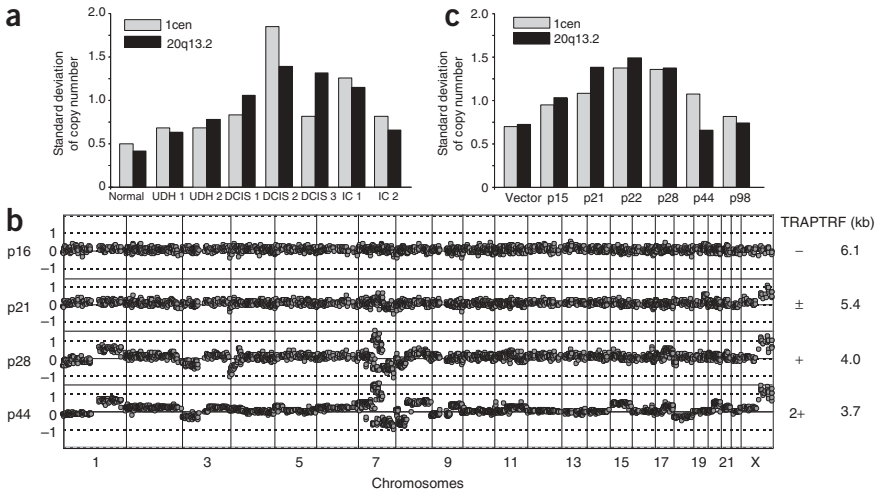

Figure 3 Genomic events measured *in vivo* and in immortalized HMECs using dual-color FISH and array CGH. (**a**) Standard deviations of 1cen and 20q13.2 copy numbers measured in normal epithelium, UDH, DCIS and invasive cancer (IC). Instability was highest in DCIS and high in invasive cancer, but somewhat lower than in DCIS. (**b**) Genome copy-number distributions measured using array CGH in *ZNF217*-immortalized HMECs[12]. $\log_2$ relative copy number (*y* axis) is plotted as a function of distance along the genome (*x* axis; 1pter on the left and chromosomes 22qter and X to the right). Vertical lines indicate chromosome boundaries. Telomerase activity and telomere lengths measured in earlier studies[12] are indicated to the right of the array CGH profiles. (**c**) Standard deviations of 1cen and 20q13.2 copy numbers measured using FISH for several passages of *ZNF217*-immortalized HMECs. Similar data was obtained for chromosomes 2p24 and 2q36 (data not shown).

© 2004 Nature Publishing Group http://www.nature.com/naturegenetics

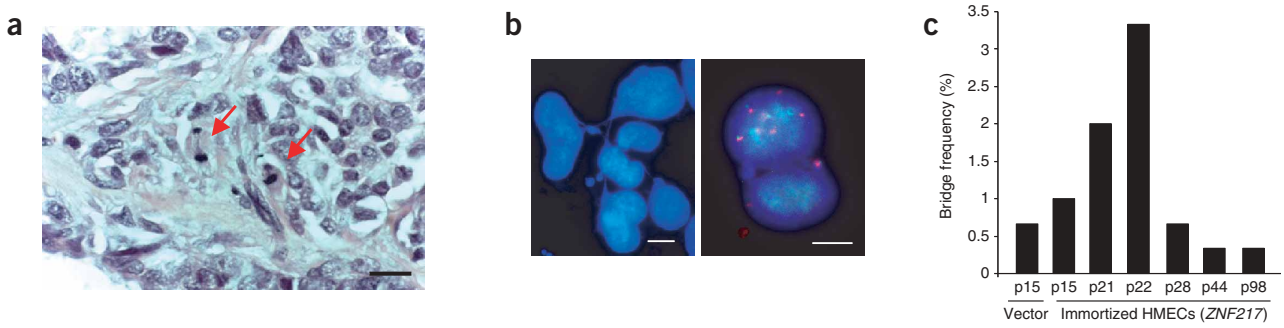

Figure 4 Anaphase bridges in human breast tumor specimens and nuclear bridges in *ZNF217*-immortalized HMECs. (**a**) Anaphase bridges in an atypical ductal hyperplasia specimen. Scale bar, 10 μm. (**b**) Left, nuclear bridges in DAPI-stained preparations of *ZNF217*-immortalized HMECs. Right, uneven partitioning at p22 of loci on chromosome 2 as indicated by FISH with probes to *MYCN* (2p24; green) and *INDPP5D* (2q36; red). Scale bars, 2.5 μm. (**c**) Nuclear bridge frequencies scored in 300 nuclei at several passages of *ZNF217*-immortalized HMECs.

© 2004 Nature Publishing Group http://www.nature.com/naturegenetics

statistical analyses showed that the nuclei with one and two copies of 1cen were randomly mixed. The nuclear volumes in all regions of UDH were similar to those measured for normal epithelial cells. One DCIS specimen had significantly higher instability (σ_{CN} = ~1–1.5; $P < 0.01$, Wilcoxon rank test; **Fig. 1e**,**f**). Cells in this sample varied substantially in genome composition and DNA content, and the number of copies of 1cen plus 20q13.2 was strongly correlated with DNA content (correlation coefficient = 0.83), indicating that the increase in DNA content was contemporaneous with the increase in genome instability. Spatial analyses of this and another specimen showed that cells with widely different chromosomal compositions were randomly mixed, indicating that most copy-number variation was due to high instability rather than clonal evolution. A third DCIS specimen had a near-normal level of instability, suggesting that it might be less far along in transition through telomere crisis. Increased 20q13.2 copy number was the dominant feature; instability was low and the nuclear volume was near normal. One invasive cancer sample had high instability, but lower than that of the DCIS specimens (σ_{CN} = ~0.67–1.28; **Fig. 2**), although the difference was not significant ($P < 0.38$, Wilcoxon rank test). Some areas (**Fig. 2b**) showed near-normal copy number and volume, whereas others (**Fig. 2c**,**d**) were highly variable in copy number and DNA content. Cells with widely different chromosomal composition were randomly mixed in most invasive cancers, although some diploid cells were spatially segregated from cells with genomic abnormalities.

We scored mitoses and anaphase bridges in thin sections stained with hematoxylin and eosin in UDH and DCIS cases adjacent to sections that were analyzed using thick-section FISH and in an additional 8 UDH cases, 12 atypical ductal hyperplasias and 11 DCIS specimens. Anaphase bridges, considered a hallmark of telomere crisis[7], were present in two atypical ductal hyperplasias and two DCIS specimens (**Fig. 4a**).

We assessed telomere length using FISH as described[10], except that we used dual-color FISH with probes to the centromeres and telomeres so that telomere length could be normalized to the centromeric hybridization intensity. The average telomere length was significantly shorter in the DCIS lesions than in normal tissue ($P < 0.03$; **Fig. 5a**), as expected, and was significantly shorter in invasive cancers than in DCIS ($P < 0.01$), even though telomerase had been reactivated. This is probably because telomere-length control acts in *cis* at each individual chromosome end, so that the critically short telomeres are stabilized but the others continue to erode[4].

We compared the genomic events that occurred during progression from UDH to invasive cancer with those that occurred in cultures of HMECs before, during and after *ZNF217*-mediated immortalization[12]. In this model, *ZNF217* transduction of HMECs with a finite lifespan allowed one or a few cells in each culture to activate telomerase, stabilize telomere length and develop resistance to transforming growth factor-β. These cells were effectively immortal and could be propagated indefinitely. In one culture, passage through

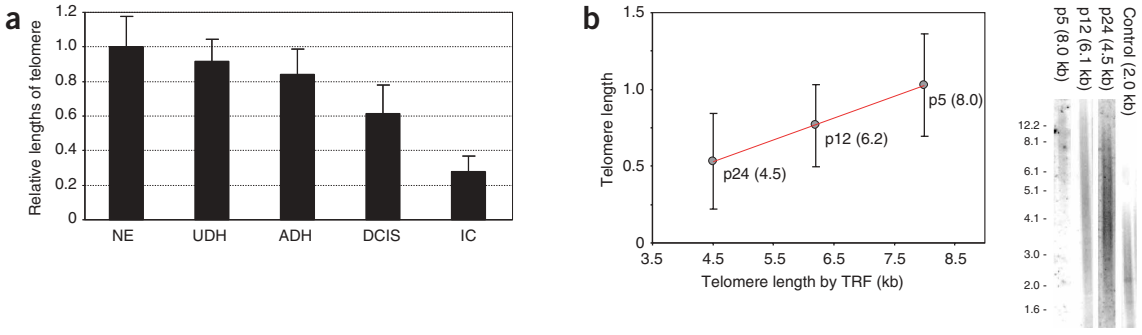

Figure 5 Relative lengths of telomeres *in vivo* and *in vitro* were assessed using dual-color FISH. (**a**) Relative lengths of telomeres in histologically defined stages of breast cancer progression: three samples of normal epithelium (NE), three samples of UDH, one sample of atypical ductal hyperplasia (ADH), five samples of DCIS and three samples of invasive cancer (IC). Error bars indicate the standard deviation of all images in each histological type. (**b**) Left, telomere length comparisons in three different passages in HMECs (prestasis finite lifespan 184, p5; post-selection finite lifespan 184, p12; and the p53-immortal line 184AA2, p24) determined using FISH (*y* axis) and the telomere restriction fragment (TRF) Southern-blot analysis (*x* axis) as described previously[26]. Right, telomere restriction fragment assays for telomere length in these cultures.

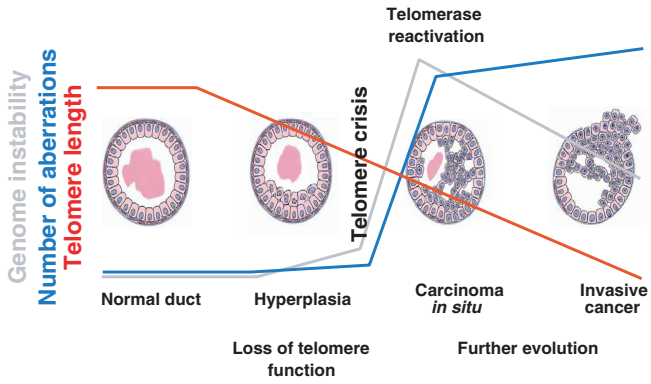

Figure 6 A schematic representation of genomic events associated with breast cancer progression. These events are generalizations from published studies and the present work describing total genomic aberrations[9,27–29], telomerase activity[11,30], telomere length[10] and genome instability. Individual tumors and lesions may vary substantially from this evolutionary pattern.

telomere crisis occurred at passage 22 (p22; **Fig. 3b,c**), as documented by maximal nuclear bridge frequency and reactivation of telomerase (**Fig. 4**). Instability was low before p22 ($\sigma_{CN} = \sim 0.6$), maximal at p22 ($\sigma_{CN} = \sim 1.5$) and significantly lower thereafter ($\sigma_{CN} = \sim 0.75$; $P < 0.04$, Wilcoxon rank test; **Fig. 3c**). Genomic aberrations detected by array CGH were not apparent before p22, increased substantially by p28 and changed slowly thereafter (**Fig. 3b**). Telomere length decreased during and after transition through telomere crisis, as observed *in vivo* (**Fig. 5b**). We obtained similar results for other cultures, but the time of passage through telomere crisis and the spectrum of genomic aberrations detected using comparative genomic hybridization (CGH) differed (data not shown).

The genomic events associated with transition through telomere crisis in *ZNF217*-transfected HMECs were remarkably similar to those observed in breast cancer during transition from UDH to DCIS (**Fig. 6**). Telomere length decreased steadily during and after transition through telomere crisis, as observed during progression from UDH to invasive cancer. Genome instability and the frequency of anaphase bridges were low before telomere crisis, as found for UDH; highest during crisis, as found for DCIS; and somewhat reduced thereafter, as found for invasive cancer. Few genome aberrations were apparent before transition, as observed in UDH; the number increased sharply shortly after telomere crisis, as found in DCIS; and the number changed slowly thereafter, as found for invasive cancer[9,14,15]. Many of the aberrations detected in post-crisis HMECs involved regions that are recurrently aberrant in primary tumors[16], suggesting that these result from active selection. Analyses of HMEC transitions though telomere crisis show that the probability of successful transition is extremely low[12]. This may explain why the risk of developing invasive cancer in individuals with UDH is only modestly increased[17].

The low probability of transition through telomere crisis also suggests that the DCIS lesions that do form arise from single cells in which telomerase is reactivated and that carry aberrations that enable further progression toward malignancy[1]. This post-transition immortal cell and its progeny would have the features ascribed to tumor stem cells[18]: active telomerase and the ability to propagate indefinitely. *In vitro* and xenograft experiments (data not shown), however, suggest that the post-transition immortal cells remain somewhat unstable and so produce the aberrant progeny detected using FISH in invasive cancers. The fact that genomically unstable cell cultures, xenografts and invasive cancers evolve slowly, as measured using CGH, suggests that the aberrant progeny are at a proliferative disadvantage relative to cells that divide normally (**Supplementary Fig. 3** online). This may explain why most apparently unstable primary and metastatic tumors evolve relatively few new genomic aberrations that can be detected using CGH.

Positioning of immortalization and telomere crisis between UDH and DCIS in breast cancer has important clinical implications. For example, assays that measure telomerase activity, genome instability and the presence of recurrent aberrations will identify lesions that have transitioned through this checkpoint and are at increased risk of further progression. In addition, agents that enhance damage surveillance[19], inhibit reactivation of telomerase[20] or poison cells with active telomerase[21] may be effective in preventing the rare UDH-to-DCIS transition and hence may be useful preventive agents.

METHODS

Tissues and sections. We cut frozen sections from three UDH cases, three DCIS specimens, four invasive cancers and two normal breast tissues, stained them with hematoxylin and eosin and examined them to identify regions of histological interest. We cut adjacent ~30-μm-thick sections attached to tape (Instrumedics), placed them on coated glass slides and attached them by polymerization through exposure to 380 nm ultraviolet irradiation for 60 s. We stored slides at –80 °C until needed.

FISH to thick tissue sections. We carried out FISH to thick sections as described previously[13] and in **Supplementary Methods** online. We mounted sections on slides, fixed them in acetone, digested them with pepsin, fixed them again in a methanol-acetone solution, air-dried them, denatured them and hybridized them for 2–3 d to denatured probes (a Cy3-labeled alpha-satellite probe (pUC1.77) for 1cen and an Alexa 568–labeled ~250-kb BAC/P1 contig containing *ZNF217* at 20q13.2) plus excess salmon sperm DNA and Cot-1 DNA. We counterstained hybridized slides with YO-PRO-1 and DAPI in antifade.

3D image acquisition. We acquired images of thick tissue sections using a laser scanning confocal microscope (Model LSM410, Carl Zeiss) equipped with a 63×, 1.3 NA plan-apo objective lens as described[22]. YO-PRO-1, Alexa568 and CY5 were excited at 488 nm, 568 nm and 633 nm, respectively, and emitted light was collected at 515–565 nm, 575–640 nm and >665 nm, respectively. We selected regions for 3D image acquisition based on histological assessment of two-dimensional (2D) YO-PRO-1 images. 3D images were typically 512 × 512 × 100 voxels and had *x*, *y*, *z* voxel dimensions of 0.2 μm, 0.2 μm and 0.3 μm, respectively.

Nuclear segmentation. We segmented the 3D images of YO-PRO-1–stained nuclei as described[22]. The 3D images were automatically divided into high (nuclear) and low (background) intensity regions and visually assessed to detect clusters of nuclei and to discard incomplete nuclei and debris. Clusters were automatically subdivided and reassessed visually. We summed the voxels comprising each segmented nucleus as an estimate of nuclear volume, which we used as an estimate of total DNA content in subsequent analyses.

Detection of FISH signals. We detected FISH signals in each segmented nucleus by applying a modified morphological top-hat method to detect high intensity, punctate signals smaller than a predefined size. We added gray-scale reconstruction to exclude signals smaller than expected for true hybridization signals and used an automatic gray-weighted threshold to select only high-intensity signals. We used Gaussian filtering before thresholding to merge closely spaced doublet signals. We used the numbers of Alexa 568 and Cy5 signals in each 3D nuclear volume as measures of the numbers of copies of 1cen and 20q13.2 in that nucleus.

Telomere length measurements. We used FISH with Cy3-labeled pan-telomeric and fluorescein isothiocyanate–labeled pan-centromeric peptide nucleic acid probes (Applied Biosystems) to label centromeres and telomeres in 5-μm-thick sections of formalin-fixed paraffin-embedded tissues. We treated deparaffi-

© 2004 Nature Publishing Group http://www.nature.com/naturegenetics

nized tissues in 1M sodium thiocyanate at 80 °C for 8 min and denatured them in 70% formamide at 73 °C for 5 min. We then washed sections, stained them with DAPI and mounted them using anti-fade buffer. We acquired Cy3, fluorescein isothiocyanate and DAPI images using a scanning confocal microscope (Zeiss LSM510). See **Supplementary Methods** online for additional details.

We used custom software to segment nuclei in regions of histological interest and to measure average centromere and telomere FISH intensities per nucleus. We estimated relative telomere length as the ratio of the total telomere signal intensity to the total centromere intensity. We analyzed at least 500 nuclei per section.

Error assessment. We assessed the accuracy of the copy number enumeration by fitting univariate copy number frequency histograms with the function

$$Prob(x \mid m,p,n) = \sum_{i=\max(n-x,0)}^{n} \binom{n}{i} \cdot (1-p)^{i} \cdot p^{(n-i)} \cdot \frac{e^{-m} \cdot m^{(x+i-n)}}{(x+i-n)!},$$

where *Prob* ($x \mid m,p,n$) is the probability of detecting x signals in a nucleus, assuming that spurious spots were Poisson-distributed with mean m, that the probability of a true genomic target being detected was p, and that there were n genuine genomic targets per nucleus.

Correlation of copy number with nuclear volume. We used linear regression analysis to assess correlations between the number of copies of 1cen and the number of copies of 20q13.2, and between the sum of the number of copies of 1cen and 20q13.2 and nuclear volume.

Anaphase bridge analysis. We scored anaphase bridges and mitoses in ten high-power fields (40× NeoFluar, Model Axioplan2, Carl Zeiss). We scored nuclear bridges in 300 nuclei of *ZNF217*-immortalized HMECs stained with DAPI as surrogates for anaphase bridges.

CGH and FISH analyses of HMECs. We grew *ZNF217*-transduced HMECs as previously described[12] and collected them at several passages for genomic analyses. We analyzed genome copy-number changes using array CGH as described previously[23]. We labeled DNAs from HMECs and normal cells with Cy3 and Cy5, respectively, and hybridized them for 2 d along with excess Cot-1 DNA to microarrays carrying BAC DNA targets distributed at ~1-Mb intervals along the genome. We stained arrays with DAPI after hybridization. We acquired DAPI, Cy3 and Cy5 images using a CCD camera system and analyzed them as described[24] to obtain relative copy number for each target. We plotted $\log_2$ Cy3:Cy5 mean intensity ratios according to location along the genome (University of California Santa Cruz human genome assembly, June 2002 freeze).

We carried out dual-color FISH analyses of HMECs using probe combinations of 1cen/20q13.2 or 2p24/2q36 as described[25]. Probes in each pair were labeled with Alexa 488 and Cy3, respectively. We scored 200 nuclei for each analysis.

Note: Supplementary information is available on the Nature Genetics website.

ACKNOWLEDGMENTS

We thank D. Pinkel and D. Albertson for discussions, advice and providing slides for array CGH; C. Thompson for advice concerning the thick-section FISH; and C. Florendo for sectioning the tissue. J.W.G. thanks F. McCormick and colleagues at Leiden University (during a Boerhave Professorship) for discussions of genome evolution in breast cancer. This work was supported by Carl Zeiss, Vysis, the Office of Health and Environmental Research of the US Department of Energy, the US National Institutes of Health, the University of California Breast Cancer Research Program and the Avon Foundation. The content of this publication does not necessarily reflect the views or policies of the Department of Health and Human Services, nor does mention of trade names, commercial products or organizations imply endorsement by the US Government.

COMPETING INTERESTS STATEMENT

The authors declare that they have no competing financial interests.

Received 26 April; accepted 1 July 2004
Published online at http://www.nature.com/naturegenetics/

1. Maser, R.S. & DePinho, R.A. Connecting chromosomes, crisis, and cancer. *Science* **297**, 565–569 (2002).
2. Hanahan, D. & Weinberg, R.A. The hallmarks of cancer. *Cell* **100**, 57–70 (2000).
3. Holst, C.R. *et al.* Methylation of p16(INK4a) promoters occurs in vivo in histologically normal human mammary epithelia. *Cancer Res.* **63**, 1596–1601 (2003).
4. Smogorzewska, A. & de Lange, T. Regulation of telomerase by telomeric proteins. *Annu. Rev. Biochem.* **73**, 177–208 (2004).
5. Romanov, S.R. *et al.* Normal human mammary epithelial cells spontaneously escape senescence and acquire genomic changes. *Nature* **409**, 633–637 (2001).
6. Artandi, S.E. *et al.* Telomere dysfunction promotes non-reciprocal translocations and epithelial cancers in mice. *Nature* **406**, 641–645 (2000).
7. Rudolph, K.L., Millard, M., Bosenberg, M.W. & DePinho, R.A. Telomere dysfunction and evolution of intestinal carcinoma in mice and humans. *Nat. Genet.* **28**, 155–159 (2001).
8. O'Hagan, R.C. *et al.* Telomere dysfunction provokes regional amplification and deletion in cancer genomes. *Cancer Cell* **2**, 149–155 (2002).
9. O'Connell, P. *et al.* Analysis of loss of heterozygosity in 399 premalignant breast lesions at 15 genetic loci. *J. Natl. Cancer Inst.* **90**, 697–703 (1998).
10. Meeker, A.K. *et al.* Telomere shortening occurs in subsets of normal breast epithelium as well as in situ and invasive carcinoma. *Am. J. Pathol.* **164**, 925–935 (2004).
11. Herbert, B.S., Wright, W.E. & Shay, J.W. Telomerase and breast cancer. *Breast Cancer Res.* **3**, 146–149 (2001).
12. Nonet, G.H. *et al.* The ZNF217 gene amplified in breast cancers promotes immortalization of human mammary epithelial cells. *Cancer Res.* **61**, 1250–1254 (2001).
13. Thompson, C.T., LeBoit, P.E., Nederlof, P.M. & Gray, J.W. Thick-section fluorescence in situ hybridization on formalin-fixed, paraffin-embedded archival tissue provides a histogenetic profile. *Am. J. Pathol.* **144**, 237–243 (1994).
14. Isola, J.J. *et al.* Genetic aberrations detected by comparative genomic hybridization predict outcome in node-negative breast cancer. *Am. J. Pathol.* **147**, 905–911 (1995).
15. Waldman, F.M. *et al.* Chromosomal alterations in ductal carcinomas in situ and their in situ recurrences. *J. Natl. Cancer Inst.* **92**, 313–320 (2000).
16. Knuutila, S., Autio, K. & Aalto, Y. Online access to CGH data of DNA sequence copy number changes. *Am. J. Pathol.* **157**, 689 (2000).
17. Dupont, W.D. & Page, D.L. Risk factors for breast cancer in women with proliferative breast disease. *N. Engl. J. Med.* **312**, 146–151 (1985).
18. Smalley, M. & Ashworth, A. Stem cells and breast cancer: A field in transit. *Nat. Rev. Cancer* **3**, 832–844 (2003).
19. Takimoto, R. *et al.* The mutant p53-conformation modifying drug, CP-31398, can induce apoptosis of human cancer cells and can stabilize wild-type p53 protein. *Cancer Biol. Ther.* **1**, 47–55 (2002).
20. Kelland, L.R. Telomerase: biology and phase I trials. *Lancet Oncol.* **2**, 95–102 (2001).
21. Kim, M.M. *et al.* A low threshold level of expression of mutant-template telomerase RNA inhibits human tumor cell proliferation. *Proc. Natl. Acad. Sci. USA* **98**, 7982–7987 (2001).
22. Ortiz de Solorzano, C. *et al.* Segmentation of confocal microscope images of cell nuclei in thick tissue sections. *J. Microsc.* **193**, 212–226 (1999).
23. Snijders, A.M. *et al.* Assembly of microarrays for genome-wide measurement of DNA copy number. *Nat. Genet.* **29**, 263–264 (2001).
24. Jain, A.N. *et al.* Fully automatic quantification of microarray image data. *Genome Res.* **12**, 325–332 (2002).
25. Kallioniemi, O.P. *et al.* ERBB2 amplification in breast cancer analyzed by fluorescence in situ hybridization. *Proc. Natl. Acad. Sci. USA* **89**, 5321–5325 (1992).
26. Allsopp, R.C. *et al.* Telomere length predicts replicative capacity of human fibroblasts. *Proc. Natl. Acad. Sci. USA* **89**, 10114–10118 (1992).
27. Nishizaki, T. *et al.* Genetic alterations in primary breast cancers and their metastases: direct comparison using modified comparative genomic hybridization. *Genes Chromosomes Cancer* **19**, 267–272 (1997).
28. Kuukasjarvi, T. *et al.* Genetic heterogeneity and clonal evolution underlying development of asynchronous metastasis in human breast cancer. *Cancer Res.* **57**, 1597–1604 (1997).
29. Kuukasjarvi, T. *et al.* Genetic changes in intraductal breast cancer detected by comparative genomic hybridization. *Am. J. Pathol.* **150**, 1465–1471 (1997).
30. Yashima, K. *et al.* Telomerase enzyme activity and RNA expression during the multistage pathogenesis of breast carcinoma. *Clin. Cancer Res.* **4**, 229–234 (1998).

© 2004 Nature Publishing Group http://www.nature.com/naturegenetics